Hindawi Publishing Corporation
International Scholarly Research Notices
Volume 2014, Article ID 312840, 16 pages
http://dx.doi.org/10.1155/2014/312840

Research Article

Effect of Stiffness on Reflection and Transmission of Waves at an Interface between Heat Conducting Elastic Solid and Micropolar Fluid Media

Rajneesh Kumar,[1] S. C. Rajvanshi,[2,3] and Mandeep Kaur[2,3]

[1] *Department of Mathematics, Kurukshetra University, Kurukshetra 136119, India*
[2] *Research Centre, Punjab Technical University, Kapurthala, India*
[3] *Department of Applied Sciences, Gurukul Vidyapeeth Institute of Engineering and Technology, Banur, Sector 7, Patiala District, Punjab 140601, India*

Correspondence should be addressed to Mandeep Kaur; mandeep1125@yahoo.com

Received 28 March 2014; Accepted 8 July 2014; Published 29 October 2014

Academic Editor: Giuseppe Maruccio

Copyright © 2014 Rajneesh Kumar et al. This is an open access article distributed under the Creative Commons Attribution License, which permits unrestricted use, distribution, and reproduction in any medium, provided the original work is properly cited.

The present investigation is concerned with the propagation of waves at an imperfect boundary of heat conducting elastic solid and micropolar fluid media. The amplitude ratios of various reflected and transmitted waves are obtained in a closed form due to incidence of longitudinal wave (P-wave), thermal wave (T-wave), and transverse wave (SV-wave). The variation of various amplitude ratios with angle of incidence is obtained for normal force stiffness, transverse force stiffness, thermal contact conductance, and perfect bonding. Numerical results are shown graphically to depict the effect of stiffness and thermal relaxation times on resulting quantities. Some particular cases are also deduced in the present investigation.

1. Introduction

The fluids in which coupling between the spin of each fluid particle and the microscopic velocity field is taken into account are termed as micropolar fluids. They represent fluids consisting of rigid, randomly oriented, or spherical particles suspended in a viscous medium, where the deformation of fluid particles is ignored. The theory of microfluids was introduced by Eringen [1]. A microfluid possesses three gyration vector fields in addition to its classical translatory degrees of freedom. As a subclass of these fluids, Eringen introduced the micropolar fluids [2] to describe the physical systems, which do not fall in the realm of viscous fluids. In micropolar fluids the local fluid elements were allowed to undergo only rigid rotations without stretch. These fluids support couple stress, the body couples, and asymmetric stress tensor and possess a rotational field, which is independent of the velocity of fluid. A large class of fluids such as anisotropic fluids, liquid crystals with rigid molecules, magnetic fluids, cloud with dust, muddy fluids, biological fluids, and dirty fluids (dusty air, snow) can be modeled more realistically as micropolar fluids. The importance of micropolar fluids in industrial applications has motivated many researchers to extend the study in numerous ways to explain various physical effects.

Ariman et al. [3, 4] studied microcontinuum fluid mechanics and its applications and Říha [5] investigated the theory of heat-conducting micropolar fluid with microtemperature. Eringen and Kafadar [6] discussed polar field theories, Brulin [7] studied linear micropolar media, Gorla [8] investigated combined forced and free convection in the boundary layer flow of a micropolar fluid on a continuous moving vertical cylinder, and Eringen [9] studied the theory of thermo-microstretch fluids and bubbly liquid. Aydemir and Venart [10] investigated flow of a thermomicropolar fluid with stretch. Ciarletta [11] established two sorts of spatial decay estimates for describing the spatial behaviour of the solutions for the flow of a heat-conducting micropolar fluid in a semi-infinite cylindrical pipe. The lateral surface is taken to be thermal insulated and the adherence of the fluid to the lateral boundary is assumed. A time-dependent velocity

and angular velocity profile are prescribed together with the temperature field at the finite end of the pipe. Hsia and Cheng [12] studied longitudinal plane waves propagation in elastic micropolar porous media. Propagation of transverse waves in elastic micropolar porous semispaces is discussed by Hsia et al. [13].

Different researchers studied the problems of reflection and transmission of plane waves at an interface of micropolar elastic half-spaces (Tomar and Gogna [14–16] and Kumar et al. [17, 18]). Singh and Tomar [19] discussed the longitudinal waves at an interface of micropolar fluid/micropolar solid half-spaces. Sun et al. [20] studied propagation characteristics of longitudinal displacement wave in micropolar fluid with micropolar elastic plate. Xu et al. [21] discussed reflection and transmission characteristics of coupled wave through micropolar elastic solid interlayer in micropolar fluid. Dang et al. [22] investigated propagation characteristics of coupled wave through micropolar fluid interlayer in micropolar elastic solid. Fu and Wei [23] investigated wave propagation through the imperfect interface between two micropolar solids. Sharma and Marin [24] studied reflection and transmission of waves from imperfect boundary between two heat conducting micropolar thermoelastic solids. Vishwakarma et al. [25] studied torsional wave propagation in an earth's crustal layer under the influence of imperfect interface.

The purpose of the present study is to study the problem of reflection and transmission of plane waves at an imperfect interface between heat conducting elastic solid and micropolar fluid media. Effects of stiffness and thermal relaxation times on the amplitude ratios for incidence of various plane waves, for example, longitudinal wave (P-wave), thermal wave (T-wave), and transverse wave (SV-wave), are depicted numerically and shown graphically with angle of incidence.

2. Basic Equations

The field equations in a homogeneous and isotropic elastic medium in the context of generalized theories of thermoelasticity, without body forces and heat sources, are given by Lord and Shulman [26] and Green and Lindsay [27] as

$$\begin{gathered}(\lambda+2\mu)\nabla(\nabla\cdot\vec{u})-\mu(\nabla\times(\nabla\times\vec{u}))\\ -\nu\left(1+\tau_1\frac{\partial}{\partial t}\right)\nabla T=\rho\frac{\partial^2\vec{u}}{\partial t^2},\\ K^*\Delta T=\rho c^*\left(\frac{\partial T}{\partial t}+\tau_0\frac{\partial^2 T}{\partial t^2}\right)+\nu T_0\left(\frac{\partial}{\partial t}+\eta_0\tau_0\frac{\partial^2}{\partial t^2}\right)(\nabla\cdot\vec{u}),\end{gathered}\tag{1}$$

and the constitutive relations are

$$\begin{gathered}t_{ij}=\lambda u_{r,r}\delta_{ij}+\mu\left(u_{i,j}+u_{j,i}\right)-\nu\left(T+\tau_1\frac{\partial T}{\partial t}\right)\delta_{ij},\\ i,j,r=1,2,3,\end{gathered}\tag{2}$$

where $\nu=(3\lambda+2\mu)\alpha_T$ and the meaning of symbols is defined in the list at the end of the paper. The thermal relaxation times τ_0 and τ_1 satisfy the inequalities $\tau_0\ge\tau_1\ge0$ for G-L theory only and $\Delta=\partial^2/\partial x_1^2+\partial^2/\partial x_3^2$ is the Laplacian operator. For Lord Shulman (L-S) theory $\eta_0=1$, $\tau_1=0$ and for Green-Lindsay (G-L) theory $\eta_0=0$, $\tau_1>0$.

Following Ciarletta [11], the field equations and the constitutive relations for heat conducting micropolar fluids without body forces, body couples, and heat sources are given by

$$\begin{gathered}D_1\vec{v}+\left(\lambda^f+\mu^f\right)\nabla(\nabla\cdot\vec{v})+K^f\left(\nabla\times\vec{\Psi}\right)-b\nabla T^f\\ -c_0\nabla\phi^{*f}=0,\end{gathered}\tag{3}$$

$$\begin{gathered}D_2\vec{\Psi}+\left(\alpha^f+\beta^f\right)\nabla\left(\nabla\cdot\vec{\Psi}\right)+K^f(\nabla\times\vec{v})=0,\\ K_1^*\Delta T^f-bT_0^f(\nabla\cdot\vec{v})=\rho^f aT_0^f\frac{\partial T^f}{\partial t},\end{gathered}\tag{4}$$

$$\rho^f\frac{\partial\phi^{*f}}{\partial t}=\nabla\cdot\vec{v},\tag{5}$$

where

$$D_1=\left(\mu^f+K^f\right)\Delta-\rho^f\frac{\partial}{\partial t},\qquad D_2=\gamma^f\Delta-I\frac{\partial}{\partial t}-2K^f,\tag{6}$$

such that superscript f denotes physical quantities and material constants related to the fluid and the constitutive relations are

$$\begin{gathered}t_{ij}^f=-p\delta_{ij}+\sigma_{ij}^f,\\ p=bT^f+c_0\phi^{*f},\\ \sigma_{ij}^f=\lambda^f\gamma_{rr}\delta_{ij}+\left(\mu^f+K^f\right)\gamma_{ij}+\mu^f\gamma_{ji},\\ m_{ij}^f=\alpha^f\upsilon_{rr}\delta_{ij}+\beta^f\upsilon_{ji}+\gamma^f\upsilon_{ij},\end{gathered}\tag{7}$$

where $\gamma_{ij}=\nu_{j,i}+\varepsilon_{jir}\Psi_r$, $\upsilon_{ij}=\Psi_{j,i}$, $b=(3\lambda^f+2\mu^f+K^f)\alpha_{T^f}$ and symbols are defined in the list at the end of the paper.

3. Formulation of the Problem

An imperfect interface of a homogeneous, isotropic generalized thermoelastic half-space (medium M_1) in contact with heat conducting micropolar fluid half-space (medium M_2) is considered. The rectangular Cartesian coordinate system $Ox_1x_2x_3$ having origin on the surface $x_3=0$ seperating the two media is taken. Let us take the x_1-axis along the interface between two half-spaces, namely, M_1 $(0<x_3<\infty)$ and M_2 $(-\infty<x_3<0)$, in such a way that x_3-axis is pointing vertically downward into the medium M_1. The geometry of the problem is shown in Figure 1.

For two dimensional problem in x_1x_3-plane, we take the displacement vector $\vec{u}$, velocity vector $\vec{v}$, and microrotation velocity vector $\vec{\Psi}$ as

$$\begin{gathered}\vec{u}=\left(u_1\left(x_1,x_3\right),0,u_3\left(x_1,x_3\right)\right),\\ \vec{v}=\left(v_1\left(x_1,x_3\right),0,v_3\left(x_1,x_3\right)\right),\qquad\vec{\Psi}=\left(0,\Psi_2\left(x_1,x_3\right),0\right).\end{gathered}\tag{8}$$

The following nondimensional quantities are defined:

$$x_i' = \frac{\omega^* x_i}{c_1}, \qquad u_i' = \frac{\rho\omega^* c_1}{\nu T_0}u_i, \qquad v_i' = \frac{\rho c_1}{\nu T_0}v_i,$$
$$\psi_2' = \frac{\rho c_1^2}{\omega^* \nu T_0}\psi_2, \qquad \left(t', \tau_0', \tau_1'\right) = \left(\omega^* t, \omega^* \tau_0, \omega^* \tau_1\right),$$
$$\left(T', T^{f\prime}\right) = \left(\frac{T}{T_0}, \frac{T^f}{T_0}\right), \qquad \left(t_{ij}', t_{ij}^{f\prime}\right) = \frac{1}{\nu T_0}\left(t_{ij}, t_{ij}^f\right),$$
$$m_{ij}^{f\prime} = \frac{\omega^*}{c_1 \nu T_0}m_{ij}^f, \qquad \phi^{*f\prime} = \rho\phi^{*f},$$
$$K_n' = \frac{c_1}{\nu T_0}K_n, \qquad K_t' = \frac{c_1}{\nu T_0}K_t, \qquad K_\theta' = \frac{1}{\nu c_1}K_\theta, \tag{9}$$

where $\omega^* = \rho c^* c_1^2/K^*$, $c_1^2 = (\lambda + 2\mu)/\rho$.

The displacement components u_1, u_3 and velocity components v_1, v_3 are related to the potential functions ϕ, ϕ^f and ψ, ψ^f in dimensionless form as

$$\begin{aligned}\left(u_1, v_1\right) &= \left(\frac{\partial}{\partial x_1}\left(\phi, \phi^f\right) - \frac{\partial}{\partial x_3}\left(\psi, \psi^f\right)\right),\\ \left(u_3, v_3\right) &= \left(\frac{\partial}{\partial x_3}\left(\phi, \phi^f\right) + \frac{\partial}{\partial x_1}\left(\psi, \psi^f\right)\right).\end{aligned} \tag{10}$$

Using (10) in (1) and (3)–(5) and with the aid of (8) and (9) (after suppressing the primes), we obtain

$$\begin{aligned}
&\nabla^2\phi - \left(1 + \tau_1\frac{\partial}{\partial t}\right)T - \frac{\partial^2\phi}{\partial t^2} = 0,\\
&\nabla^2\psi - a_1\frac{\partial^2\psi}{\partial t^2} = 0,\\
&\nabla^2 T = \left(1 + \tau_0\frac{\partial}{\partial t}\right)\frac{\partial T}{\partial t} + \varepsilon_1\left(\frac{\partial}{\partial t} + \eta_0\tau_0\frac{\partial^2}{\partial t^2}\right)\nabla^2\phi,\\
&\nabla^2\phi^f - b_1 T^f - b_2\phi^{*f} - b_3\frac{\partial\phi^f}{\partial t} = 0,\\
&\nabla^2\psi^f + b_4\Psi_2 - b_5\frac{\partial\psi^f}{\partial t} = 0,\\
&\nabla^2 T^f - b_9\nabla^2\phi^f - b_{10}\frac{\partial T^f}{\partial t} = 0,\\
&\nabla^2\Psi_2 - b_6\nabla^2\psi^f - b_7\Psi_2 - b_8\frac{\partial\Psi_2}{\partial t} = 0,\\
&b_{11}\nabla^2\phi^f - \frac{\partial}{\partial t}\phi^{*f} = 0,
\end{aligned} \tag{11}$$

where

$$a_1 = \frac{\rho c_1^2}{\mu}, \qquad \varepsilon_1 = \frac{\nu^2 T_0}{K^*\omega^*\rho}, \qquad b_1 = \frac{b\rho c_1^2}{\left(\lambda^f + 2\mu^f + K^f\right)\omega^*\nu},$$
$$b_2 = \frac{c_0 c_1^2}{\left(\lambda^f + 2\mu^f + K^f\right)\omega^*\nu T_0},$$
$$b_3 = \frac{\rho^f c_1^2}{\left(\lambda^f + 2\mu^f + K^f\right)\omega^*}, \qquad b_4 = \frac{K^f}{\mu^f + K^f},$$
$$b_5 = \frac{\rho^f c_1^2}{\left(\mu^f + K^f\right)\omega^*}, \qquad b_6 = \frac{K^f c_1^2}{\gamma^f\omega^{*2}},$$
$$b_7 = 2b_6, \qquad b_8 = \frac{I c_1^2}{\gamma^f\omega^*}, \qquad b_9 = \frac{b\nu T_0^f}{K_1^*\rho\omega^*},$$
$$b_{10} = \frac{\rho^f a T_0^f c_1^2}{K_1^*\omega^*}, \qquad b_{11} = \frac{\nu T_0}{\rho^f c_1^2}. \tag{12}$$

4. Boundary Conditions

The boundary conditions at the interface $x_3 = 0$ are defined as

$$t_{33}^f = K_n\left(\frac{\partial u_3}{\partial t} - v_3\right), \qquad t_{31}^f = K_t\left(\frac{\partial u_1}{\partial t} - v_1\right),$$
$$K_1^*\frac{\partial T^f}{\partial x_3} = K_\theta\left(T - T^f\right), \qquad t_{33} = t_{33}^f, \qquad t_{31} = t_{31}^f,$$
$$m_{32}^f = 0, \qquad K^*\frac{\partial T}{\partial x_3} = K_1^*\frac{\partial T^f}{\partial x_3}, \tag{13}$$

where K_n, K_t, and K_θ are the normal force stiffness, transverse force stiffness, and thermal contact conductance coefficients of unit layer thickness having dimensions $\mathrm{N\,sec/m^3}$, $\mathrm{N\,sec/m^3}$, and $\mathrm{N/m\,sec\,K}$.

5. Reflection and Transmission

The longitudinal wave (P-wave) or thermal wave (T-wave) or transverse wave (SV-wave) propagating through the medium M_1 which is designated as the region $x_3 > 0$ is considered. The plane wave is taken to be incident at the plane $x_3 = 0$ with its direction of propagation with angle θ_0 normal to the surface. Each incident wave corresponds to reflected P-wave, T-wave, and SV-wave in medium M_1 and transmitted longitudinal wave (L-wave), thermal wave (T-wave), and transverse longitudinal wave coupled with transverse microrotational wave (C-I and C-II waves) in medium M_2 as shown in Figure 1.

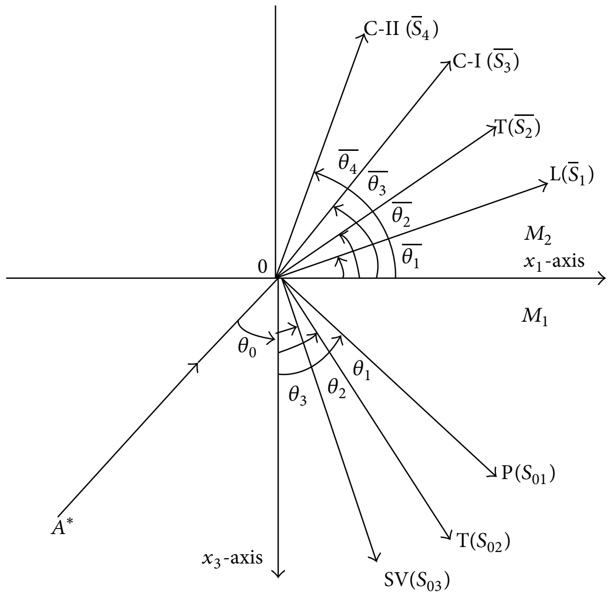

Figure 1: Geometry of the problem.

In order to solve (11), we assume the solutions of the system of the form

$$\left\{\phi, T, \psi, \phi^f, \phi^{*f}, T^f, \psi^f, \Psi_2\right\} = \left\{\overline{\phi}, \overline{T}, \overline{\psi}, \overline{\phi^f}, \overline{\phi^{*f}}, \overline{T^f}, \overline{\psi^f}, \overline{\Psi_2}\right\} e^{\iota\{k(x_1 \sin\theta - x_3 \cos\theta) - \omega t\}}, \tag{14}$$

where k is the wave number, ω is the angular frequency, and $\overline{\phi}, \overline{T}, \overline{\psi}, \overline{\phi^f}, \overline{\phi^{*f}}, \overline{T^f}, \overline{\psi^f}, \overline{\Psi_2}$ are arbitrary constants.

Making use of (14) in (11), we obtain

$$V^4 + D_1 V^2 + E_1 = 0, \tag{15}$$

$$\begin{gathered} V^4 + D_2 V^2 + E_2 = 0, \\ V^4 + D_3 V^2 + E_3 = 0, \end{gathered} \tag{16}$$

where

$$\begin{gathered} D_1 = -\frac{1}{\tau_{00}} \left[1 + (1 - \iota\tau_1\omega)\,\varepsilon_1 \left(\frac{\iota}{\omega} + \eta_0\tau_0\right)\right] - 1, \\ E_1 = \frac{1}{\tau_{00}}, \\ D_2 = \frac{\iota\omega}{b_3}\left(1 - \frac{\iota b_2 b_{11}}{\omega}\right) + \frac{\iota\omega}{b_{10}}\left(1 + \frac{\iota b_1 b_9}{\omega b_3}\right), \\ E_2 = \frac{-\omega^2}{b_3 b_{10}}\left(1 - \frac{\iota b_2 b_{11}}{\omega}\right), \\ D_3 = \frac{\iota\omega}{b_5} + \iota\omega\left[\frac{(1 - \iota b_4 b_6/\omega b_5)}{(b_8 + (\iota/\omega)\, b_7)}\right], \\ E_3 = -\frac{\omega^2}{(b_8 + (\iota/\omega)\, b_7)\, b_5}, \\ V^2 = \frac{\omega^2}{k^2}, \qquad \tau_{00} = \left(\frac{\iota}{\omega} + \tau_0\right). \end{gathered} \tag{17}$$

Here V_1, V_2 are the velocities of P-wave and T-wave in medium M_1 and these are roots of (15) and $V_3 = 1/\sqrt{a_1}$ is the velocity of SV-wave in medium M_1. $\overline{V_1}$, $\overline{V_2}$, $\overline{V_3}$, and $\overline{V_4}$ are the velocities of transmitted longitudinal wave (L-wave), thermal wave (T-wave), and transverse longitudinal wave coupled with microrotational wave (C-I and C-II) in medium M_2. These are roots of (16).

In view of (14), the appropriate solutions of (11) for medium M_1 and medium M_2 are taken as follows.

Medium M_1 is as follows:

$$\begin{gathered} \{\phi, T\} = \sum_{i=1}^{2} \{1, f_i\} \left[S_{0i} e^{\iota\{k_i(x_1 \sin\theta_{0i} - x_3 \cos\theta_{0i}) - \omega_i t\}} + P_i\right], \\ \psi = S_{03} e^{\iota\{k_3(x_1 \sin\theta_{03} - x_3 \cos\theta_{03}) - \omega_3 t\}} + S_3 e^{\iota\{k_3(x_1 \sin\theta_{03} + x_3 \cos\theta_{03}) - \omega_3 t\}}, \end{gathered} \tag{18}$$

where

$$\begin{gathered} f_i = \frac{\varepsilon_1 \omega_i^2 (\iota/\omega_i + \eta_0\tau_0)}{-1/V_i^2 + (\iota/\omega_i + \tau_0) - \iota\varepsilon_1\omega_i (\iota/\omega_i + \eta_0\tau_0)(\iota/\omega_i + \tau_1)}, \\ P_i = S_i e^{\iota\{k_i(x_1 \sin\theta_i + x_3 \cos\theta_i) - \omega_i t\}}. \end{gathered} \tag{19}$$

Medium M_2 is as follows:

$$\left\{\phi^f, T^f, \phi^{*f}\right\} = \sum_{i=1}^{2} \left\{1, \overline{f_i}, \overline{g_i}\right\} \overline{S_i} e^{\iota\{\overline{k_i}(x_1 \sin\overline{\theta_i} - x_3 \cos\overline{\theta_i}) - \overline{\omega_i} t\}}, \tag{20}$$

$$\left\{\psi^f, \Psi_2\right\} = \sum_{j=3}^{4} \left\{1, \overline{f_j}\right\} \overline{S_j} e^{\iota\{\overline{k_j}(x_1 \sin\overline{\theta_j} - x_3 \cos\overline{\theta_j}) - \overline{\omega_j} t\}}, \tag{21}$$

where

$$\begin{gathered} \overline{f_i} = \frac{-b_3 b_9}{b_1 b_9 (\iota/\omega_i) + \iota\omega_i (1 - \iota b_2 b_{11}/\omega_i)\left(1/\overline{V_i}^2 - b_{10}(\iota/\omega_i)\right)}, \\ \overline{f_j} = \frac{(b_6 b_5 (\iota/\omega_i))}{-1/\overline{V_j}^2 - b_7/\omega_j^2 + b_8 (\iota/\omega_i) + b_4 b_6/\omega_j^2}, \qquad \overline{g_i} = \frac{-\iota b_{11}\omega_i}{\overline{V_i}^2}, \end{gathered} \tag{22}$$

and S_{0i}, S_{03} are the amplitudes of incident (P-wave, T-wave) and SV-wave, respectively. S_i and S_3 are the amplitudes of reflected (P-wave, T-wave) and SV-wave and $\overline{S_i}$, $\overline{S_j}$ are the amplitudes of transmitted longitudinal wave, thermal wave,

and transverse longitudinal wave coupled with transverse microrotational wave, respectively.

Equation (20) represents the relation between (ϕ^f and T^f) and (ϕ^f and ϕ^{f*}).

Snell's law is given by

$$\frac{\sin\theta_0}{V_0} = \frac{\sin\theta_1}{V_1} = \frac{\sin\theta_2}{V_2} = \frac{\sin\theta_3}{V_3} = \frac{\sin\overline{\theta_1}}{\overline{V_1}} = \frac{\sin\overline{\theta_2}}{\overline{V_2}} = \frac{\sin\overline{\theta_3}}{\overline{V_3}} = \frac{\sin\overline{\theta_4}}{\overline{V_4}}, \tag{23}$$

where

$$k_1V_1 = k_2V_2 = k_3V_3 = \overline{k_1}\,\overline{V_1} = \overline{k_2}\,\overline{V_2} = \overline{k_3}\,\overline{V_3} = \overline{k_4}\,\overline{V_4} = \omega, \quad \text{at } x_3 = 0. \tag{24}$$

Making use of (18)–(21) in the boundary conditions (13) and with the help of (2), (7), (9), (10), (23), and (24), we obtain a system of seven nonhomogeneous equations which can be written as

$$\sum_{j=1}^{7} a_{ij}Z_j = Y_i; \quad (i = 1, 2, 3, 4, 5, 6, 7), \tag{25}$$

where the values of a_{ij} are given in the Appendix.

(1) For incident P-wave,

$$A^* = S_{01}, \quad S_{02} = S_{03} = 0, \quad Y_1 = a_{11}, \quad Y_2 = -a_{21}, \quad Y_3 = -a_{31}, \quad Y_4 = -a_{41}, \quad Y_5 = a_{51}, \quad Y_6 = 0, \quad Y_7 = a_{71}. \tag{26}$$

(2) For incident T-wave,

$$A^* = S_{02}, \quad S_{01} = S_{03} = 0, \quad Y_1 = a_{12}, \quad Y_2 = -a_{22}, \quad Y_3 = -a_{32}, \quad Y_4 = -a_{42}, \quad Y_5 = a_{52}, \quad Y_6 = 0, \quad Y_7 = a_{72}. \tag{27}$$

(3) For incident SV-wave,

$$A^* = S_{03}, \quad S_{01} = S_{02} = 0, \quad Y_1 = -a_{13}, \quad Y_2 = a_{23}, \quad Y_3 = a_{33} = 0, \quad Y_4 = -a_{43}, \quad Y_5 = -a_{53}, \quad Y_6 = 0, \quad Y_7 = a_{73} = 0,$$
$$Z_1 = \frac{S_1}{A^*}, \quad Z_2 = \frac{S_2}{A^*}, \quad Z_3 = \frac{S_3}{A^*}, \quad Z_4 = \frac{\overline{S_1}}{A^*}, \quad Z_5 = \frac{\overline{S_2}}{A^*}, \quad Z_6 = \frac{\overline{S_3}}{A^*}, \quad Z_7 = \frac{\overline{S_4}}{A^*}, \tag{28}$$

where Z_1, Z_2, and Z_3 are the amplitude ratios of reflected P-wave, T-wave, and SV-wave in medium M_1 and Z_4, Z_5, Z_6, and Z_7 are the amplitude ratios of transmitted longitudinal wave (L-wave), thermal wave (T-wave), and transverse longitudinal wave coupled with transverse microrotational wave (C-I and C-II waves) in medium M_2.

6. Particular Cases

6.1. Case I: Normal Force Stiffness. $K_n \neq 0$, $K_t \to \infty$, and $K_\theta \to \infty$ in (25) yield the resulting quantities for normal force stiffness and lead a system of seven nonhomogeneous equations given by (A.1) with the changed values of a_{ij} as

$$a_{2i} = -\frac{\omega^2}{V_0}\sin\theta_0, \quad a_{23} = \frac{\omega^2}{V_3}\sqrt{1 - \frac{V_3^2}{V_0^2}\sin^2\theta_0},$$
$$a_{24} = \iota\frac{\omega}{V_0}\sin\theta_0, \quad a_{25} = \iota\frac{\omega}{V_0}\sin\theta_0,$$
$$a_{26} = \iota\frac{\omega}{\overline{V_3}}\sqrt{1 - \frac{\overline{V_3^2}}{V_0^2}\sin^2\theta_0}, \quad a_{27} = \iota\frac{\omega}{\overline{V_4}}\sqrt{1 - \frac{\overline{V_4^2}}{V_0^2}\sin^2\theta_0},$$
$$a_{3i} = f_i, \quad a_{33} = 0, \quad a_{34} = -\overline{f_1},$$
$$a_{35} = -\overline{f_2}, \quad a_{36} = a_{37} = 0. \tag{29}$$

6.2. Case II: Transverse Force Stiffness. $K_t \neq 0$, $K_n \to \infty$, and $K_\theta \to \infty$ in (25) provide the case of transverse force stiffness giving a system of seven nonhomogeneous equations given by (A.1) with the changed values of a_{ij} as

$$a_{1i} = -\frac{\omega^2}{V_i}\sqrt{1 - \frac{V_i^2}{V_0^2}\sin^2\theta_0},$$
$$a_{13} = -\frac{\omega^2}{V_0}\sin\theta_0, \quad a_{14} = -\left\{\iota\frac{\omega}{\overline{V_1}}\left(\sqrt{1 - \frac{\overline{V_1^2}}{V_0^2}\sin^2\theta_0}\right)\right\},$$
$$a_{15} = -\left\{\iota\frac{\omega}{\overline{V_2}}\left(\sqrt{1 - \frac{\overline{V_2^2}}{V_0^2}\sin^2\theta_0}\right)\right\}, \quad a_{16} = \iota\frac{\omega}{V_0}\sin\theta_0,$$
$$a_{17} = \iota\frac{\omega}{V_0}\sin\theta_0, \quad a_{3i} = f_i, \quad a_{33} = 0,$$
$$a_{34} = -\overline{f_1}, \quad a_{35} = -\overline{f_2}, \quad a_{36} = a_{37} = 0. \tag{30}$$

6.3. Case III: Thermal Contact Conductance. Taking $K_\theta \neq 0$, $K_t \to \infty$, and $K_n \to \infty$ in (25) corresponds to the case of thermal contact conductance and yields a system of

seven nonhomogeneous equations as given by (A.1) with the changed values of a_{ij} as

$$a_{1i} = -\frac{\omega^2}{V_i}\sqrt{1-\frac{V_i^2}{V_0^2}\sin^2\theta_0}, \qquad a_{13} = -\frac{\omega^2}{V_0}\sin\theta_0,$$

$$a_{14} = -\left\{\iota\frac{\omega}{\overline{V_1}}\left(\sqrt{1-\frac{\overline{V_1^2}}{V_0^2}\sin^2\theta_0}\right)\right\},$$

$$a_{15} = -\left\{\iota\frac{\omega}{\overline{V_2}}\left(\sqrt{1-\frac{\overline{V_2^2}}{V_0^2}\sin^2\theta_0}\right)\right\},$$

$$a_{16} = a_{17} = \iota\frac{\omega}{V_0}\sin\theta_0, \qquad a_{2i} = -\frac{\omega^2}{V_0}\sin\theta_0, \tag{31}$$

$$a_{23} = \frac{\omega^2}{V_3}\sqrt{1-\frac{V_3^2}{V_0^2}\sin^2\theta_0}, \qquad a_{24} = \iota\frac{\omega}{V_0}\sin\theta_0,$$

$$a_{25} = \iota\frac{\omega}{V_0}\sin\theta_0, \qquad a_{26} = \iota\frac{\omega}{\overline{V_3}}\sqrt{1-\frac{\overline{V_3^2}}{V_0^2}\sin^2\theta_0},$$

$$a_{27} = \iota\frac{\omega}{\overline{V_4}}\sqrt{1-\frac{\overline{V_4^2}}{V_0^2}\sin^2\theta_0}.$$

6.4. Case IV: Perfect Bonding. If we take $K_n \to \infty$, $K_t \to \infty$, and $K_\theta \to \infty$ in (25), we obtain the case of perfect bonding and yield a system of seven nonhomogeneous equations as given by (A.1) with the changed values of a_{ij} as

$$a_{1i} = -\frac{\omega^2}{V_i}\sqrt{1-\frac{V_i^2}{V_0^2}\sin^2\theta_0}, \qquad a_{13} = -\frac{\omega^2}{V_0}\sin\theta_0,$$

$$a_{14} = -\left\{\iota\frac{\omega}{\overline{V_1}}\left(\sqrt{1-\frac{\overline{V_1^2}}{V_0^2}\sin^2\theta_0}\right)\right\},$$

$$a_{15} = -\left\{\iota\frac{\omega}{\overline{V_2}}\left(\sqrt{1-\frac{\overline{V_2^2}}{V_0^2}\sin^2\theta_0}\right)\right\},$$

$$a_{16} = a_{17} = \iota\frac{\omega}{V_0}\sin\theta_0, \qquad a_{2i} = -\frac{\omega^2}{V_0}\sin\theta_0,$$

$$a_{23} = \frac{\omega^2}{V_3}\sqrt{1-\frac{V_3^2}{V_0^2}\sin^2\theta_0}, \qquad a_{24} = \iota\frac{\omega}{V_0}\sin\theta_0,$$

$$a_{25} = \iota\frac{\omega}{V_0}\sin\theta_0, \qquad a_{26} = \iota\frac{\omega}{\overline{V_3}}\sqrt{1-\frac{\overline{V_3^2}}{V_0^2}\sin^2\theta_0},$$

$$a_{27} = \iota\frac{\omega}{\overline{V_4}}\sqrt{1-\frac{\overline{V_4^2}}{V_0^2}\sin^2\theta_0}, \qquad a_{3i} = f_i,$$

$$a_{33} = 0, \qquad a_{34} = -\overline{f_1}, \qquad a_{35} = -\overline{f_2}, \qquad a_{36} = a_{37} = 0. \tag{32}$$

6.5. Subcases

(i) If micropolar heat conducting fluid medium is absent, we obtain the amplitude ratios at the free surface of thermoelastic solid with one relaxation time and two relaxation times.

These results are similar to those obtained by A. N. Sinha and S. B. Sinha [28] for one relaxation time (L-S theory) and Sinha and Elsibai [29] for two relaxation times (G-L theory).

(ii) In the absence of upper medium M_2, we obtain the amplitude ratios at the free surface of thermoelastic solid for CT-theory ($\eta_0 = \tau_0 = \tau_1 = 0$).

These results are similar to those obtained by Deresiewicz [30] for CT-theory.

7. Special Cases

(i) If $\eta_0 = 1$, $\tau_1 = 0$ in (25), (A.1), (29), (30), and (31) then we obtain the corresponding amplitude ratios at an interface of thermoelastic solid with one relaxation time and heat conducting micropolar fluid half-space for normal force stiffness, transverse force stiffness, and thermal contact conductance.

(ii) If $\eta_0 = 0$, $\tau_1 > 0$ in (25), (A.1), (29), (30), and (31) then we obtain the corresponding amplitude ratios at an interface of thermoelastic solid with two relaxation times and heat conducting micropolar fluid half-space for normal force stiffness, transverse force stiffness, and thermal contact conductance.

8. Numerical Results and Discussion

The following values of relevant parameters for both the half-spaces for numerical computations are taken.

Following Singh and Tomar [19], the values of elastic constants for medium M_1 are taken as

$$\lambda = 0.209730 \times 10^{10}\,\mathrm{Nm^{-2}}, \qquad \mu = 0.91822 \times 10^{9}\,\mathrm{Nm^{-2}},$$
$$\rho = 0.0034 \times 10^{3}\,\mathrm{Kg\,m^{-3}}, \tag{33}$$

and thermal parameters are taken from Dhaliwal and Singh [31]:

$$\nu = 0.268 \times 10^7 \text{ Nm}^{-2}\text{ K}^{-1},$$
$$c^* = 1.04 \times 10^3 \text{ Nm Kg}^{-1}\text{ K}^{-1},$$
$$K^* = 1.7 \times 10^2 \text{ N sec}^{-1}\text{ K}^{-1}, \qquad T_0 = 0.298 \text{ K}, \tag{34}$$
$$\tau_0 = 0.613 \times 10^{-12} \text{ sec}, \qquad \tau_1 = 0.813 \times 10^{-12} \text{ sec},$$
$$\omega = 1.$$

Following Singh and Tomar [19], the values of micropolar constants for medium M_2 are taken as

$$\lambda^f = 1.5 \times 10^8 \text{ N sec m}^{-2}, \quad \mu^f = 0.03 \times 10^8 \text{ N sec m}^{-2},$$
$$K^f = 0.000223 \times 10^8 \text{ N sec m}^{-2}, \qquad \gamma^f = 0.0000222 \text{ N sec},$$
$$\rho^f = 0.8 \times 10^3 \text{ Kg m}^{-3}, \qquad I = 0.00400 \times 10^{-16} \text{ N sec}^2\text{ m}^{-2}. \tag{35}$$

Thermal parameters for the medium M_2 are taken as of comparable magnitude:

$$T_0^f = 0.196 \text{ K}, \qquad K_1^* = 0.89 \times 10^2 \text{ N sec}^{-1}\text{ K}^{-1},$$
$$c_0 = 0.005 \times 10^{11} \text{ N sec}^2\text{ m}^{-6},$$
$$a = 1.5 \times 10^5 \text{ m}^2\text{ sec}^{-2}\text{ K}^{-2}, \qquad b = 1.6 \times 10^5 \text{ Nm}^{-2}\text{ K}^{-1}. \tag{36}$$

The values of amplitude ratios have been computed at different angles of incidence.

In Figures 2–22, for L-S theory, we represent the solid line for stiffness (ST1), small dashes line for normal force stiffness (NS1), medium dashes line for transverse force stiffness (TS1), and dash dot dash line for thermal contact conductance (TCS1). For G-L theory, we represent the dash double dot dash line for stiffness (ST2), solid line with center symbol "plus" for normal force stiffness (NS2), solid line with center symbol "diamond" for transverse force stiffness (TS2), and solid line with center symbol "cross" for thermal contact conductance (TCS2).

8.1. P-Wave Incident. Variations of amplitude ratios $|Z_i|$, $1 \leq i \leq 7$, with the angle of incidence θ_0, for incident P-wave are shown in Figures 2–8.

Figure 2 shows that the values of $|Z_1|$ for NS1 and NS2 increase in the whole range. The values for ST1, ST2, transverse force stiffness, and thermal contact conductance decrease in the whole range, except near the grazing incidence, where the values get increased. The values for ST1 remain more than the values for TS1, TS2, ST2, TCS1, and TCS2 in the whole range.

From Figure 3 it is evident that the values of $|Z_2|$ for all the stiffnesses, except ST1 and ST2, decrease in the whole range. The values of $|Z_2|$ for NS1 and NS2 are magnified by multiplying by 10.

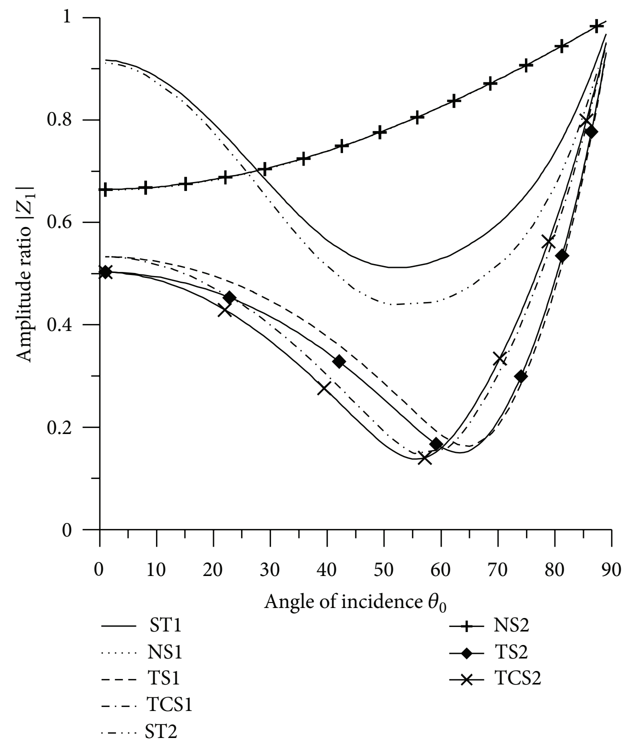

FIGURE 2: Variation of $|Z_1|$ with angle of incidence (P-wave).

Figure 4 shows that the values of $|Z_3|$ for all the stiffnesses for L-S theory and G-L theory first increase up to intermediate range and then decrease with the increase in θ_0 and the values for ST2 are greater than the values for ST1, NS1, NS2, TS1, TS2, TCS1, and TCS2 in the whole range. The values of $|Z_2|$ for NS1 and NS2 are magnified by multiplying by 10.

From Figure 5 it is noticed that the values of $|Z_4|$ for all the stiffnesses start with maximum value at normal incidence and then decrease to attain minimum value at grazing incidence. The values of amplitude ratios for ST1 and NS1 are more than the values for ST2 and NS2, respectively, in the whole range. There is slight difference in the values of TCS1 and TCS2 in the whole range. The values of $|Z_4|$ for ST1, ST2, NS1, and NS2 are magnified by multiplying by 10^2 and the values for TS1, TS2, TCS1, and TCS2 are magnified by multiplying by 10.

Figure 6 shows that the values of $|Z_5|$ for all the boundary stiffnesses decrease with increase in θ and the values of amplitude ratio for TS1 are greater than the values for all other boundary stiffnesses in the whole range that shows the effect of transverse force stiffness. The values of $|Z_5|$ for all the stiffnesses are magnified by multiplying by 10^2.

From Figure 7 it is evident that the amplitude of $|Z_6|$ for normal force stiffness increases in the range $0^\circ < \theta_0 < 48^\circ$ and then decreases in the further range. The values for transverse force stiffness increase in the range $0^\circ < \theta_0 < 59^\circ$ and for thermal contact conductance increase in the range $0^\circ < \theta_0 < 56^\circ$ and then decrease. The values of $|Z_6|$ for all the stiffnesses, except TCS1 and TCS2, are magnified by

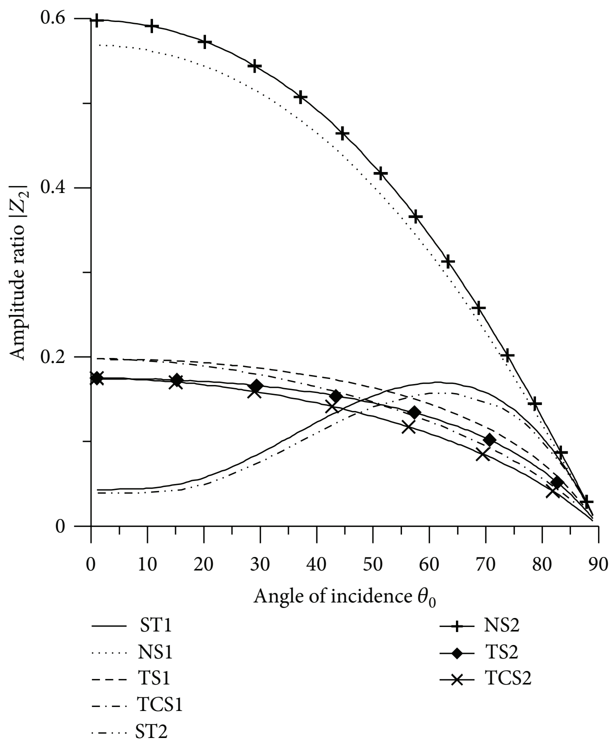

FIGURE 3: Variation of $|Z_2|$ with angle of incidence (P-wave).

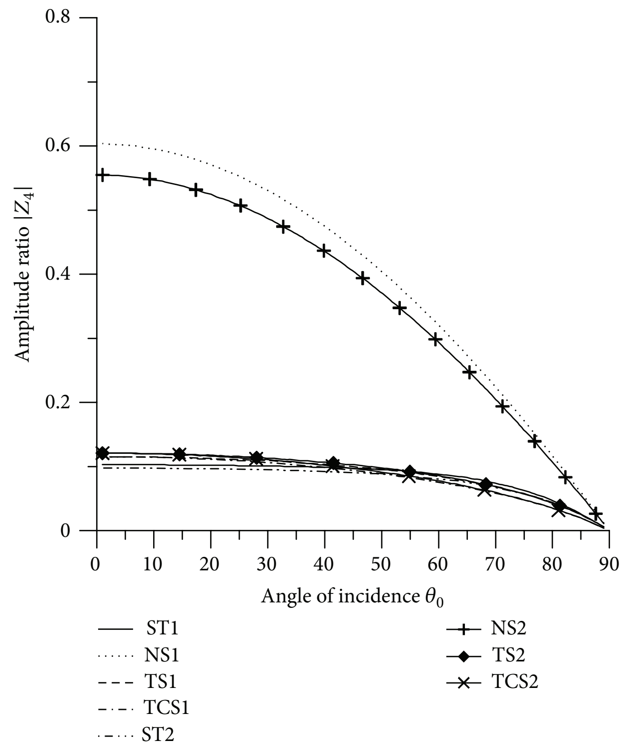

FIGURE 5: Variation of $|Z_4|$ with angle of incidence (P-wave).

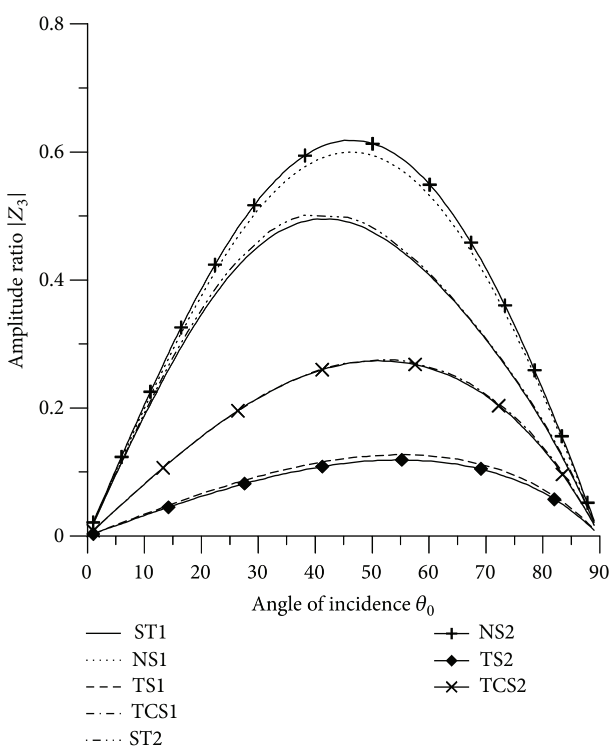

FIGURE 4: Variation of $|Z_3|$ with angle of incidence (P-wave).

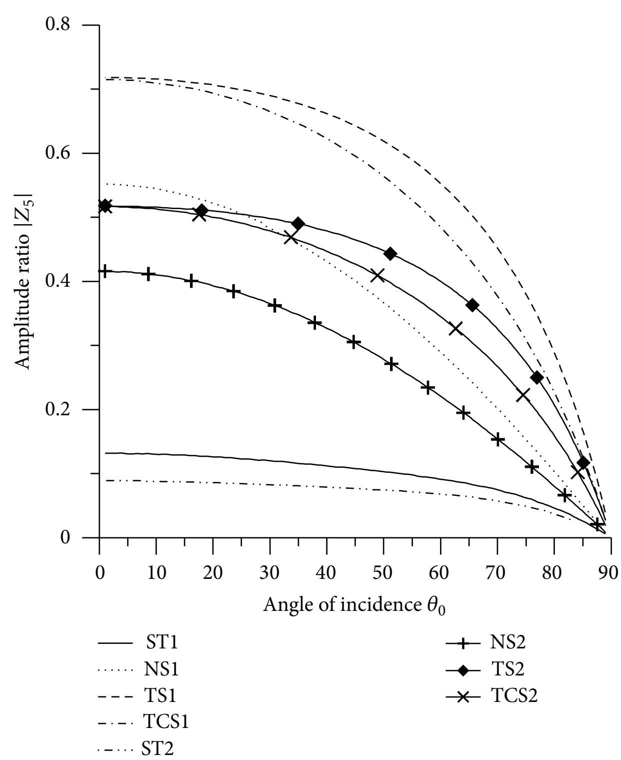

FIGURE 6: Variation of $|Z_5|$ with angle of incidence (P-wave).

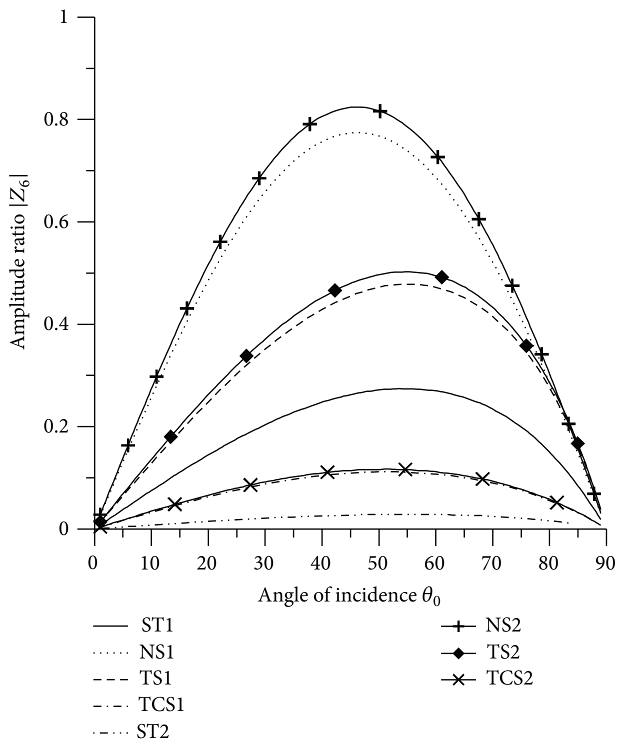

Figure 7: Variation of $|Z_6|$ with angle of incidence (P-wave).

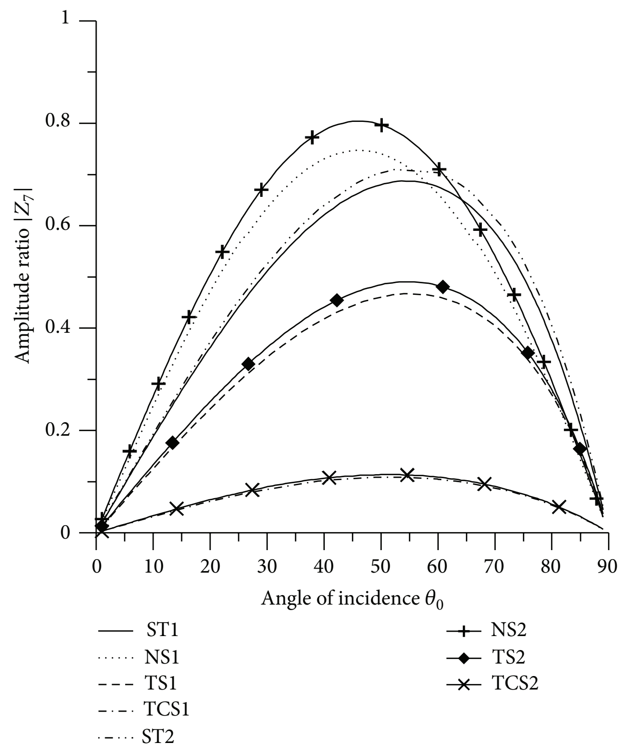

Figure 8: Variation of $|Z_7|$ with angle of incidence (P-wave).

multiplying by 10^3, while the values for TCS1 and TCS2 are magnified by multiplying by 10^2.

Figure 8 depicts that the values of $|Z_7|$ for ST1, ST2, TS1 and TS2 increase in the range $0^\circ < \theta_0 < 56^\circ$ and decrease in the remaining range. The values for ST2 and TS2 are greater than the values for ST1 and TS2 respectively in the whole range. The values for normal force stiffness for G-L theory remain more than the values for L-S theory. The values of $|Z_7|$ for ST1, ST2 are magnified by multiplying by 10^8, the values for TCS1, TCS2 are magnified by multiplying by 10^6 and the values for NS1, NS2, TS1 and TS2 are magnified by multiplying by 10^7.

8.2. T-Wave Incident. The values of amplitude ratio $|Z_1|$ for transverse force stiffness and thermal contact conductance decrease in the whole range with slight increase in the initial range. The values for ST1 and ST2 increase in the range $0^\circ < \theta_0 < 48^\circ$ and then decrease. These variations have been shown in Figure 9. The values for TS1, TS2, TCS1 and TCS2 are reduced by dividing by 10.

The values of amplitude ratio $|Z_2|$ for NS1 and NS2 increase in the whole range, while the values for TS1, TS2, ST1, ST2, TCS1, TCS2 first decrease and then increase to attain maximum value at grazing incidence. These variations are shown in Figure 10.

From Figure 11, it is noticed that the values of $|Z_3|$ for normal force stiffness, transverse force stiffness, and thermal contact conductance for G-L theory are greater than the corresponding values for L-S theory. It is seen that the values for ST1 are greater than the values for ST2 in the range $0^\circ < \theta_0 < 38^\circ$ and, in the further range, the values for ST2 are more.

Figure 12 depicts that the values of amplitude ratios $|Z_4|$ for transverse force stiffness and thermal contact conductance oscillate up to intermediate range and then decrease in the further range to attain minimum value at grazing incidence. The values for ST1, ST2, NS1, and NS2 decrease in the whole range. The values of $|Z_4|$ for ST1 and ST2 are magnified by multiplying by a factor of 10^2 and NS1, NS2, TS1, TS2, TCS1, and TCS2 are magnified by a factor of 10.

Figure 13 shows that the behavior of variation of $|Z_5|$ for all the boundary stiffnesses is similar to that of $|Z_4|$, but the magnitude of variation is different. The values of $|Z_5|$ for ST1 and ST2 are magnified by multiplying by a factor of 10^2 and NS1, NS2, TS1, TS2, TCS1, and TCS2 are magnified by a factor of 10.

From Figure 14 it is evident that the values of $|Z_6|$ for all the boundary stiffnesses increase to attain maximum value and then decrease up to grazing incidence. The values for NS1 and TS1 are greater than the values for NS2 and TS2, respectively, that reveals the thermal relaxation time effect. The values of $|Z_5|$ for ST1 and ST2 are magnified by multiplying by a factor of 10^3 and NS1, NS2, TS1, TS2, TCS1, and TCS2 are magnified by a factor of 10^2.

Figure 15 depicts that the values of $|Z_7|$ for ST1 and ST2 increase in the interval $0^\circ < \theta_0 < 39^\circ$ and then decrease in the further range. It is noticed that there is slight difference in the values of amplitude ratio for L-S and G-L theory.

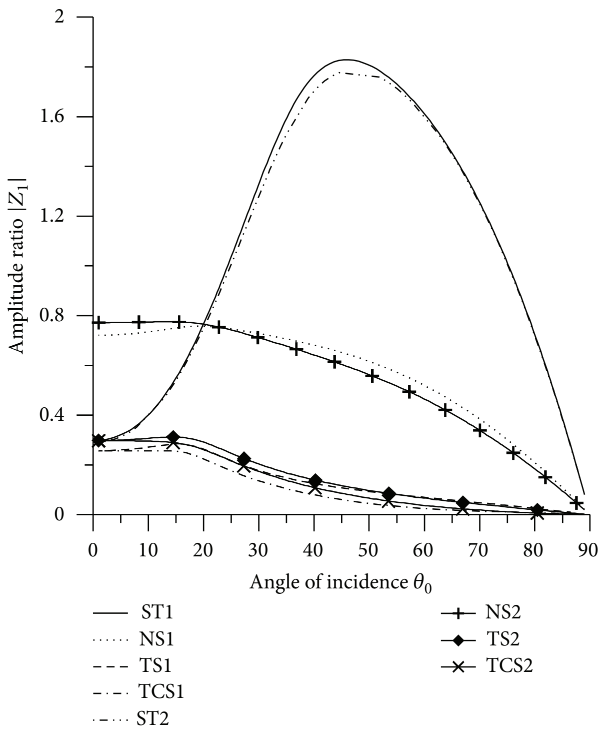

Figure 9: Variation of $|Z_1|$ with angle of incidence (P-wave).

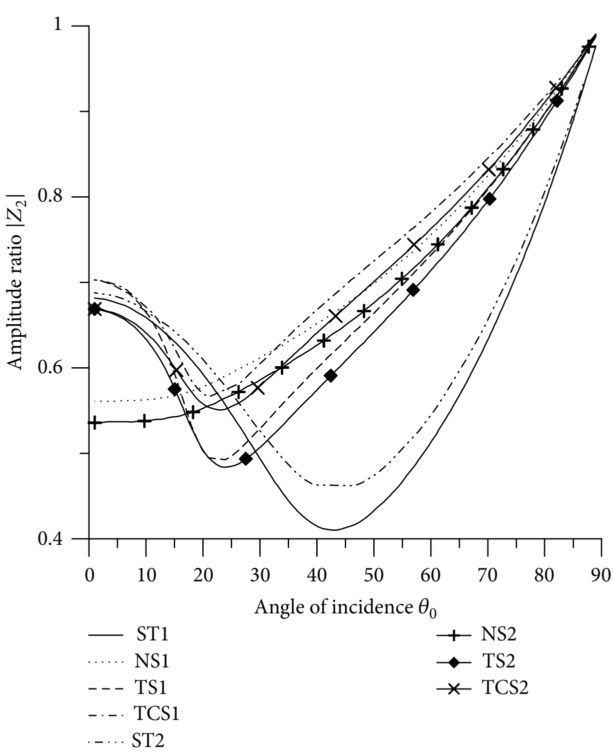

Figure 10: Variation of $|Z_2|$ with angle of incidence (P-wave).

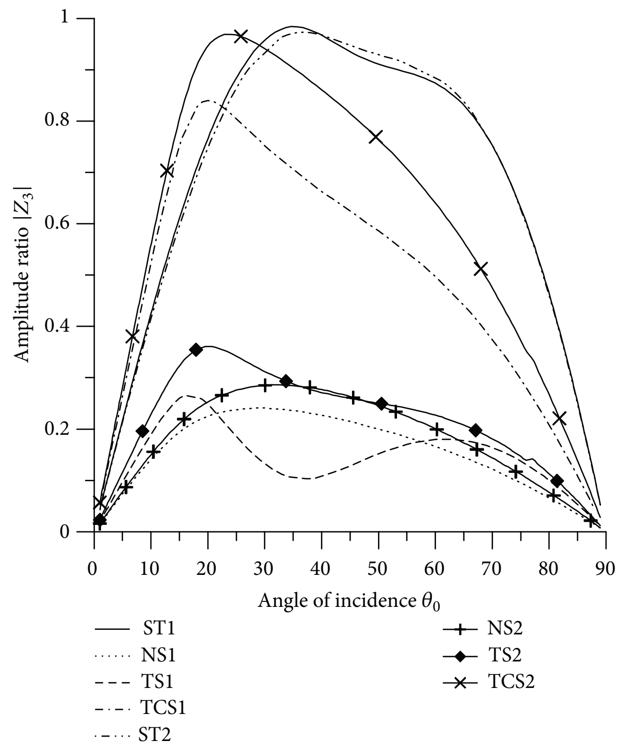

Figure 11: Variation of $|Z_3|$ with angle of incidence (T-wave).

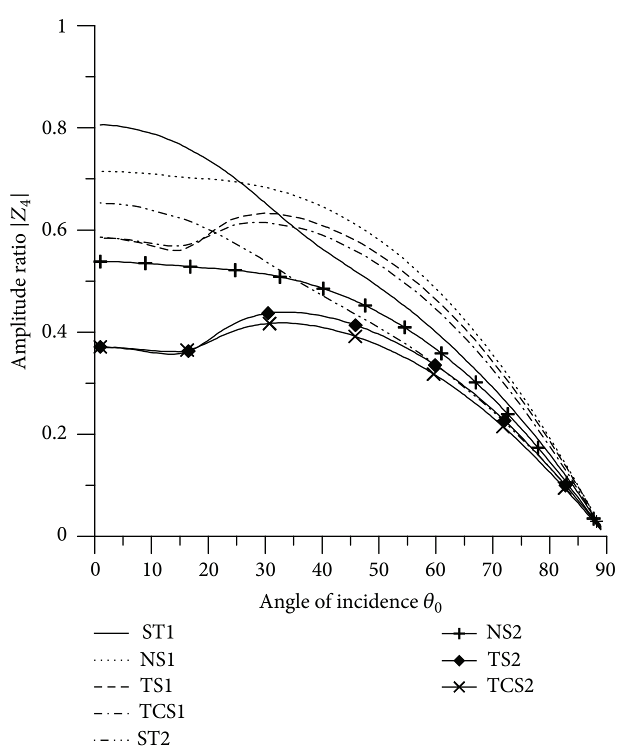

Figure 12: Variation of $|Z_4|$ with angle of incidence (T-wave).

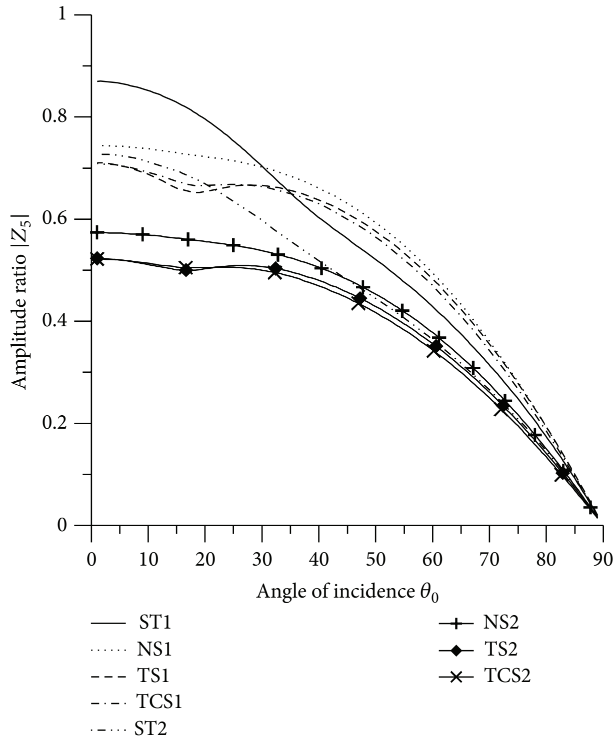

FIGURE 13: Variation of $|Z_5|$ with angle of incidence (T-wave).

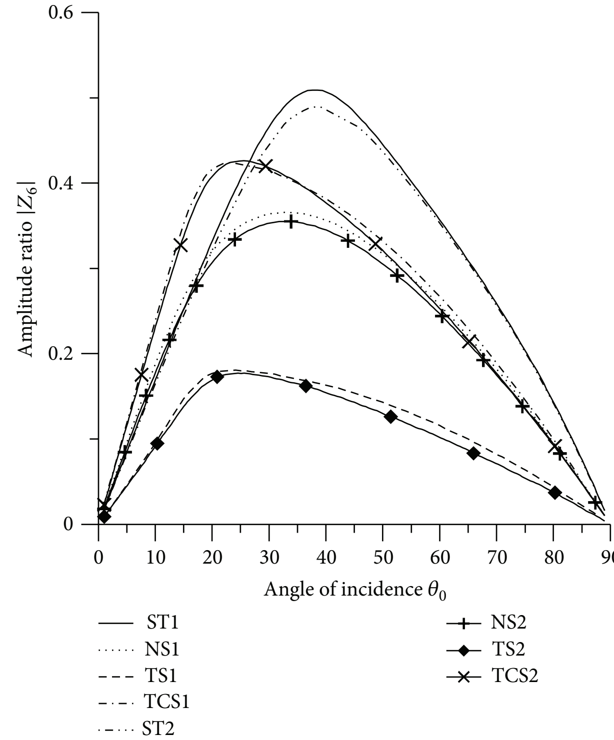

FIGURE 14: Variation of $|Z_6|$ with angle of incidence (T-wave).

The values of $|Z_7|$ for ST1 and ST2 are magnified by multiplying by a factor of 10^8 and NS1, NS2, TS1, TS2, TCS1, and TCS2 are magnified by a factor of 10^6.

8.3. SV Wave Incident. Variations of amplitude ratios $|Z_i|$, $1 \leq i \leq 7$, with the angle of incidence θ_0, for incident SV-wave are shown in Figures 16–22.

Figure 16 depicts that the values of $|Z_1|$ for transverse force stiffness and thermal contact conductance increase to attain peak values in the range $15^\circ < \theta_0 < 25^\circ$ and then decrease in the further range. The values for ST1 and ST2 increase in the range $0^\circ < \theta_0 < 35^\circ$ and $45^\circ < \theta_0 < 66^\circ$, respectively, and decrease in the remaining range. The values for normal force stiffness increase from normal incidence to attain maximum value in the range $45^\circ < \theta_0 < 55^\circ$ and then decrease up to grazing incidence. The values for TS1, TS2, TCS1, and TCS2 are reduced by dividing by 10.

Figure 17 shows that values of amplitude ratio $|Z_2|$ for all the boundary stiffnesses follow oscillatory pattern in the whole range. The maximum value is attained by TCS1 in the range $15^\circ < \theta_0 < 25^\circ$. It is seen that the values for L-S theory are greater than the values for G-L theory in the whole range.

Figure 18 shows that the values of $|Z_3|$ for transverse force stiffness increase from normal incidence to grazing incidence and attain peak value in the interval $15^\circ < \theta_0 < 25^\circ$. The values for normal stiffness and thermal contact conductance decrease in the intervals $0^\circ < \theta_0 < 56^\circ$ and $0^\circ < \theta_0 < 17^\circ$, respectively, and then increase in the further range.

Figure 19 shows that the values of $|Z_4|$ for all the boundary stiffnesses oscillate in the whole range. The values for ST1 are greater than the values for ST2 in the whole range, except some intermediate range. The values of $|Z_4|$ for ST1 and ST2 are magnified by multiplying by a factor of 10^3 and NS1, NS2, TS1, and TS2 by a factor of 10^2 and TCS1 and TCS2 are magnified by a factor of 10.

Figure 20 depicts that the behavior of variation of $|Z_5|$ for all the boundary stiffnesses is similar to that of $|Z_4|$, but the magnitude of variation is different. The values of $|Z_5|$ for ST1, ST2 are magnified by multiplying by a factor of 10^3 and NS1, NS2, TCS1, TCS2, TS1, and TS2 are magnified by a factor of 10^2.

From Figure 21, it is noted that the values of $|Z_6|$ for ST1 and ST2 decrease in the range $0^\circ < \theta_0 < 45^\circ$and then increase with increase in angle of incidence. The values of amplitude ratio for transverse force stiffness and thermal contact conductance decrease in the whole range, except the ranges $16^\circ < \theta_0 < 24^\circ$ and $17^\circ < \theta_0 < 23^\circ$, respectively. The amplitude ratio for normal force stiffness attains maximum value at normal incidence. The values of $|Z_6|$ for ST1, ST2 are magnified by multiplying by a factor of 10^3 and NS1, NS2, TCS1, TCS2, TS1, and TS2 are magnified by a factor of 10^2.

Figure 22 depicts that the values of $|Z_7|$ for all the boundary stiffnesses attain maximum value at the normal incidence and then decrease with oscillation to attain minimum value at the grazing incidence. The values of $|Z_7|$ for ST1 and ST2 are magnified by multiplying by a factor of 10^8 and NS1, NS2, TS1, TS2, TCS1, and TCS2 are magnified by a factor of 10^6.

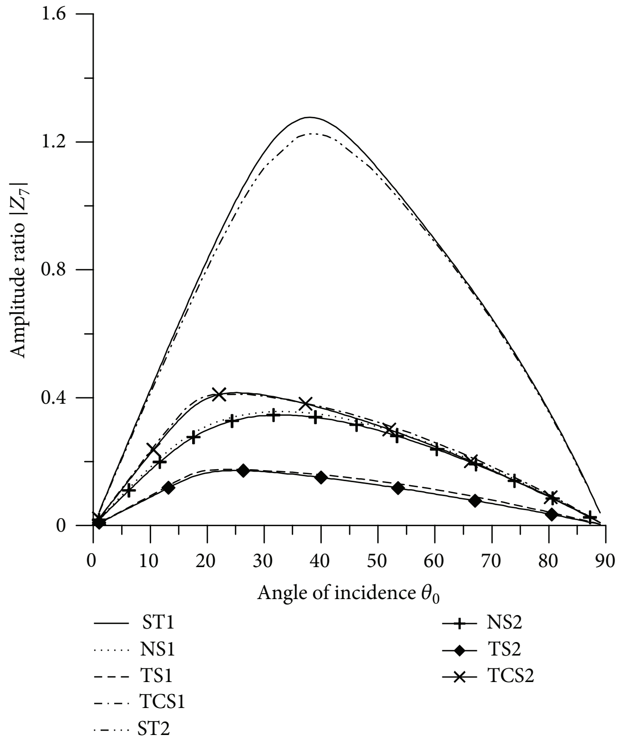

FIGURE 15: Variation of $|Z_7|$ with angle of incidence for T-wave.

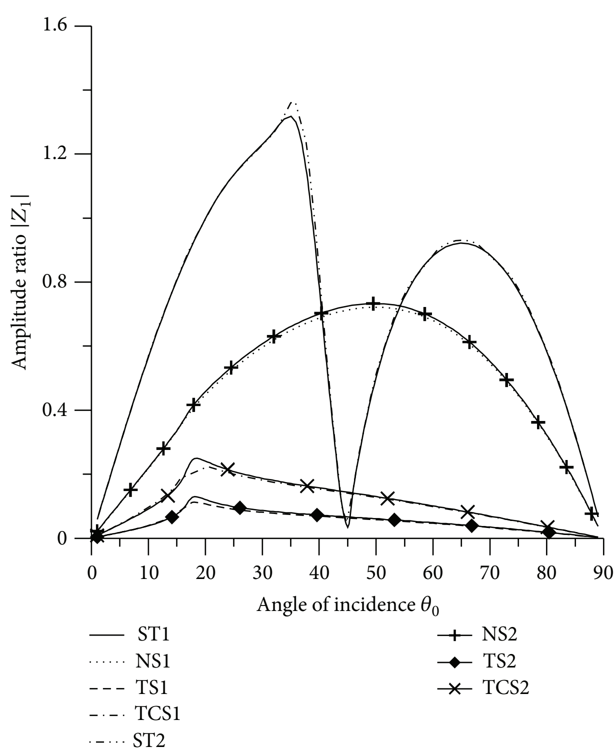

FIGURE 16: Variation of $|Z_1|$ with angle of incidence (SV-wave).

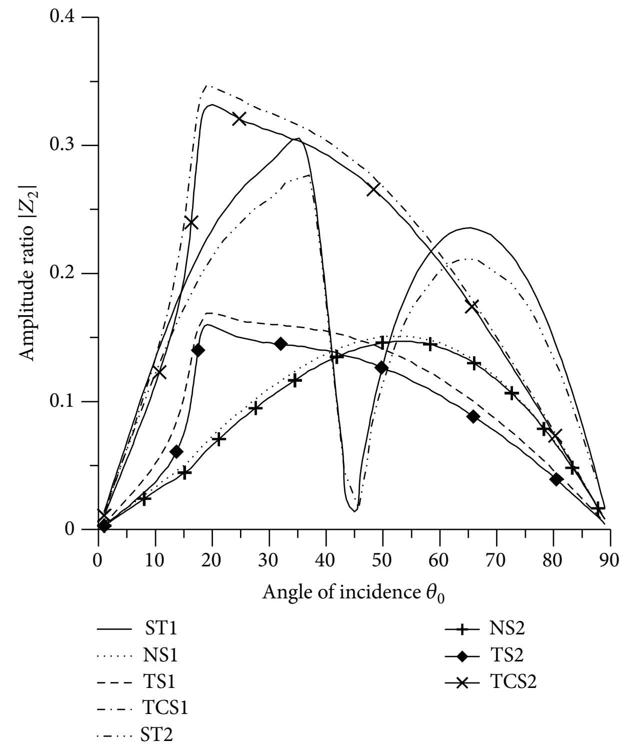

FIGURE 17: Variation of $|Z_2|$ with angle of incidence (SV-wave).

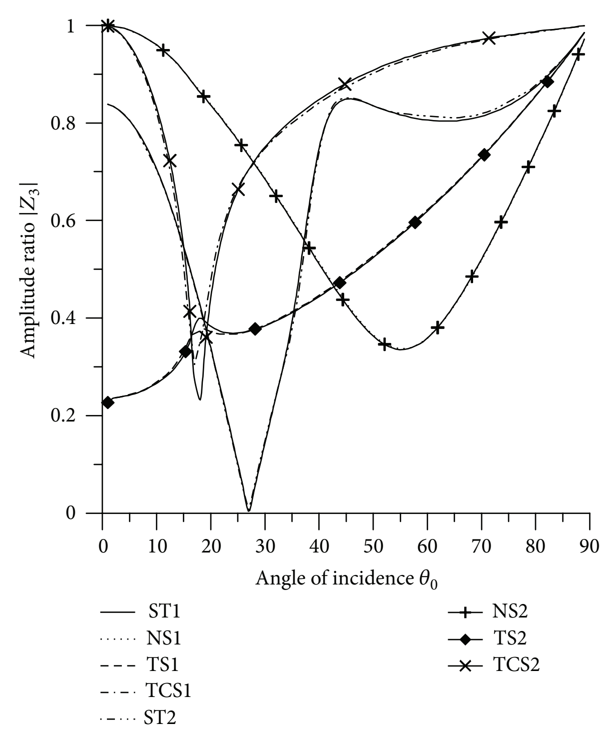

FIGURE 18: Variation of $|Z_3|$ with angle of incidence (SV-wave).

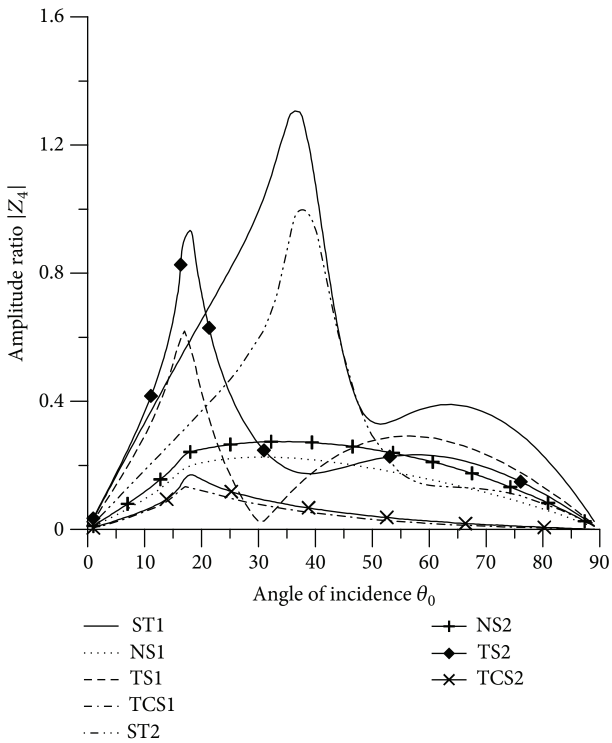

FIGURE 19: Variation of $|Z_4|$ with angle of incidence (SV-wave).

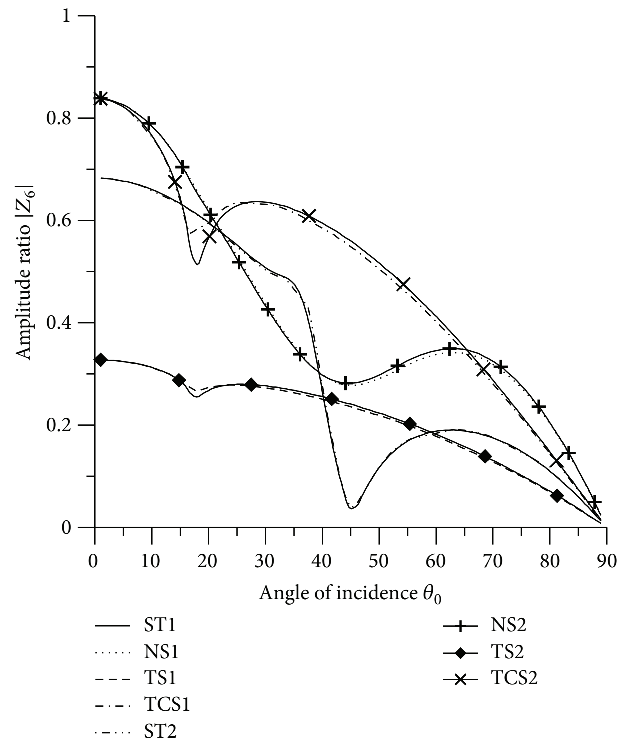

FIGURE 21: Variation of $|Z_6|$ with angle of incidence (SV-wave).

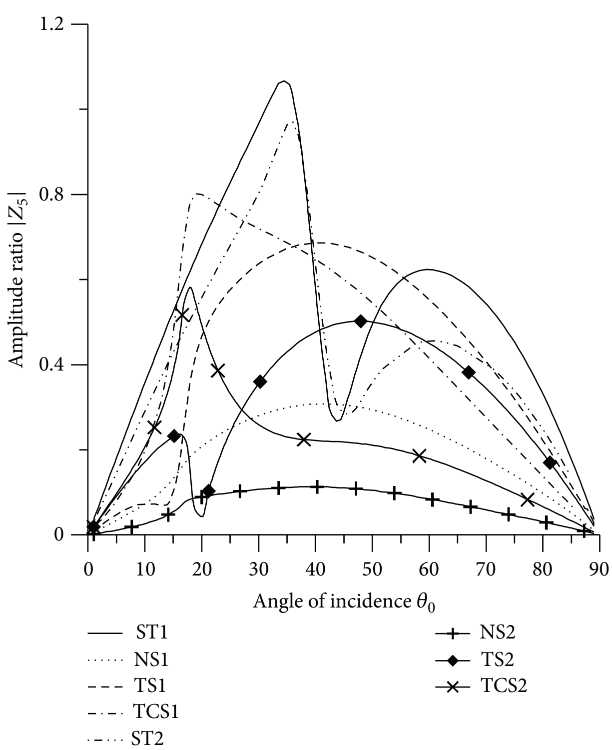

FIGURE 20: Variation of $|Z_5|$ with angle of incidence (SV-wave).

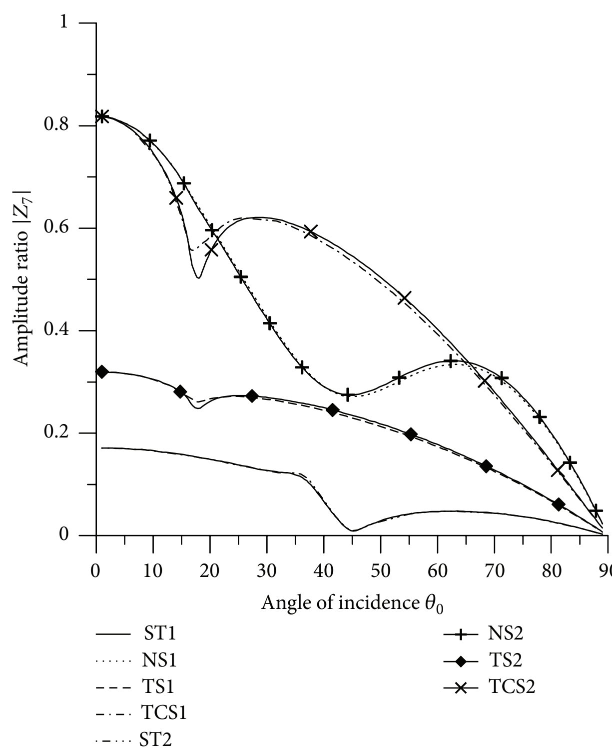

FIGURE 22: Variation of $|Z_7|$ with angle of incidence (SV-wave).

9. Conclusion

Reflection and transmission at an interface between heat conducting elastic solid and micropolar fluid media are discussed in the present paper. Effect of normal force stiffness, transverse force stiffness, thermal contact conductance, and thermal relaxation times is observed on the amplitude ratios for incidence of various plane waves (P-wave, T-wave, and SV-wave). When P-wave is incident, it is noticed that the values of amplitude ratio for transverse force stiffness for transmitted T-wave are greater than all the other boundary stiffnesses. When plane wave (SV-wave) is incident, the trend of variation of amplitude ratio for transmitted transverse wave coupled with transverse microrotational wave, that is, C-I and C-II waves, is similar, but magnitude of oscillation is different. The values of amplitude ratio of transmitted LD-wave and T-wave for L-S theory are greater than the value for G-L theory (when T-wave is incident). The model considered is one of the more realistic forms of earth models and it may be of interest for experimental seismologists in exploration of valuable materials such as minerals and crystal metals.

Appendix

Consider the following:

$$a_{1i} = -c_1 K_n \frac{\omega^2}{V_i}\sqrt{1-\frac{V_i^2}{V_0^2}\sin^2\theta_0}, \qquad a_{13} = -c_1 K_n \frac{\omega^2}{V_0}\sin\theta_0,$$

$$a_{14} = -\left\{\left[d_2^f + d_3^f\left(1-\frac{\overline{V_1^2}}{V_0^2}\sin^2\theta_0\right)\right]\frac{\omega^2}{\overline{V_1^2}} + d_1^{ff}\overline{f_1} + \overline{g_1}d_1^f + \iota c_1 K_n \frac{\omega}{\overline{V_1}}\left(\sqrt{1-\frac{\overline{V_1^2}}{V_0^2}\sin^2\theta_0}\right)\right\},$$

$$a_{15} = -\left\{\left[d_2^f + d_3^f\left(1-\frac{\overline{V_2^2}}{V_0^2}\sin^2\theta_0\right)\right]\frac{\omega^2}{\overline{V_2^2}} + d_1^{ff}\overline{f_1} + \overline{g_2}d_1^f + \iota c_1 K_n \frac{\omega}{\overline{V_2}}\left(\sqrt{1-\frac{\overline{V_2^2}}{V_0^2}\sin^2\theta_0}\right)\right\},$$

$$a_{16} = d_3^f \frac{\omega^2}{\overline{V_3}V_0}\sin\theta_0\sqrt{1-\frac{\overline{V_3^2}}{V_0^2}\sin^2\theta_0} + \iota c_1 K_n \frac{\omega}{V_0}\sin\theta_0,$$

$$a_{17} = d_3^f \frac{\omega^2}{\overline{V_4}V_0}\sin\theta_0\sqrt{1-\frac{\overline{V_4^2}}{V_0^2}\sin^2\theta_0} + \iota c_1 K_n \frac{\omega}{V_0}\sin\theta_0,$$

$$a_{2i} = -c_2 K_t \frac{\omega^2}{V_0}\sin\theta_0, \qquad a_{23} = c_2 K_t \frac{\omega^2}{V_3}\sqrt{1-\frac{V_3^2}{V_0^2}\sin^2\theta_0},$$

$$a_{24} = \left(2d_4^f + d_5^f\right)\frac{\omega^2}{\overline{V_1}V_0}\sin\theta_0\sqrt{1-\frac{\overline{V_1^2}}{V_0^2}\sin^2\theta_0} + \iota c_2 K_t \frac{\omega}{V_0}\sin\theta_0,$$

$$a_{25} = \left(2d_4^f + d_5^f\right)\frac{\omega^2}{\overline{V_2}V_0}\sin\theta_0\sqrt{1-\frac{\overline{V_2^2}}{V_0^2}\sin^2\theta_0} + \iota c_2 K_t \frac{\omega}{V_0}\sin\theta_0,$$

$$a_{26} = d_4^f \frac{\omega^2}{\overline{V_3^2}}\left(1-2\frac{\overline{V_3^2}}{V_0^2}\sin^2\theta_0\right) + d_5^f\left[\sqrt{1-\frac{\overline{V_3^2}}{V_0^2}\sin^2\theta_0} - \overline{f_3}\right] + \iota c_2 K_t \frac{\omega}{\overline{V_3}}\sqrt{1-\frac{\overline{V_3^2}}{V_0^2}\sin^2\theta_0},$$

$$a_{27} = d_4^f \frac{\omega^2}{\overline{V_4^2}}\left(1-2\frac{\overline{V_4^2}}{V_0^2}\sin^2\theta_0\right) + d_5^f\left[\sqrt{1-\frac{\overline{V_4^2}}{V_0^2}\sin^2\theta_0} - \overline{f_4}\right] + \iota c_2 K_t \frac{\omega}{\overline{V_4}}\sqrt{1-\frac{\overline{V_4^2}}{V_0^2}\sin^2\theta_0},$$

$$a_{3i} = c_4 K_\theta f_i, \qquad a_{33} = 0,$$

$$a_{34} = \left[\iota\frac{\omega}{\overline{V_1}}\sqrt{1-\frac{\overline{V_1^2}}{V_0^2}\sin^2\theta_0} - c_4 K_\theta\right]\overline{f_1},$$

$$a_{35} = \left[\iota\frac{\omega}{\overline{V_2}}\sqrt{1-\frac{\overline{V_2^2}}{V_0^2}\sin^2\theta_0} - c_4 K_\theta\right]\overline{f_2}, \qquad a_{36} = a_{37} = 0,$$

$$a_{4i} = \left(d_1 + d_2\left(1-\frac{V_i^2}{V_0^2}\sin^2\theta_0\right)\right)\frac{\omega^2}{V_i^2} + \left(1-\tau_1\iota\omega\right)f_i,$$

$$a_{43} = d_2\frac{\omega^2}{V_3 V_0}\sin\theta_0\sqrt{1-\frac{V_3^2}{V_0^2}\sin^2\theta_0},$$

$$a_{44} = -\left[\left(d_2^f + d_3^f\left(1-\frac{\overline{V_1^2}}{V_0^2}\sin^2\theta_0\right)\right)\frac{\omega^2}{\overline{V_1^2}} + \left(d_1^{ff}\overline{f_1} + d_1^f\overline{g_1}\right)\right],$$

$$a_{45} = -\left[\left(d_2^f + d_3^f\left(1-\frac{\overline{V_2^2}}{V_0^2}\sin^2\theta_0\right)\right)\frac{\omega^2}{\overline{V_2^2}} + \left(d_1^{ff}\overline{f_1} + d_1^f\overline{g_1}\right)\right],$$

$$a_{46} = d_3^f\frac{\omega^2}{\overline{V_3}V_0}\sin\theta_0\sqrt{1-\frac{\overline{V_3^2}}{V_0^2}\sin^2\theta_0},$$

$$a_{47} = d_3^f \frac{\omega^2}{\overline{V_4} V_0} \sin\theta_0 \sqrt{1 - \frac{\overline{V_4^2}}{V_0^2}\sin^2\theta_0},$$

$$a_{51} = -\left(2d_4\right) \frac{\omega^2}{V_1 V_0} \sin\theta_0 \sqrt{1 - \frac{V_1^2}{V_0^2}\sin^2\theta_0},$$

$$a_{52} = -\left(2d_4\right) \frac{\omega^2}{V_2 V_0} \sin\theta_0 \sqrt{1 - \frac{V_2^2}{V_0^2}\sin^2\theta_0},$$

$$a_{53} = d_4 \frac{\omega^2}{V_3^2} \left(1 - 2\frac{V_3^2}{V_0^2}\sin^2\theta_0\right),$$

$$a_{54} = -\left(2d_4^f + d_5^f\right) \frac{\omega^2}{\overline{V_1} V_0} \sin\theta_0 \sqrt{1 - \frac{\overline{V_1^2}}{V_0^2}\sin^2\theta_0},$$

$$a_{55} = -\left(2d_4^f + d_5^f\right) \frac{\omega^2}{\overline{V_2} V_0} \sin\theta_0 \sqrt{1 - \frac{\overline{V_2^2}}{V_0^2}\sin^2\theta_0},$$

$$a_{56} = -\left[d_4^f \frac{\omega^2}{\overline{\overline{V_3^2}}} \left(1 - 2\frac{\overline{V_3^2}}{V_0^2}\sin^2\theta_0\right) + d_5^f \left(\frac{\omega^2}{\overline{\overline{V_3^2}}} \left(\sqrt{1 - \frac{\overline{V_3^2}}{V_0^2}\sin^2\theta_0} \right) - \overline{f_3} \right) \right],$$

$$a_{57} = -\left[d_4^f \frac{\omega^2}{\overline{\overline{V_4^2}}} \left(1 - 2\frac{\overline{V_4^2}}{V_0^2}\sin^2\theta_0\right) + d_5^f \left(\frac{\omega^2}{\overline{\overline{V_4^2}}} \left(\sqrt{1 - \frac{\overline{V_4^2}}{V_0^2}\sin^2\theta_0} \right) - \overline{f_4} \right) \right],$$

$$a_{6i} = a_{63} = a_{64} = a_{65} = 0,$$

$$a_{66} = \iota \frac{\omega}{\overline{V_3}} \overline{f_3} \sqrt{1 - \frac{\overline{V_3^2}}{V_0^2}\sin^2\theta_0},$$

$$a_{67} = \iota \frac{\omega}{\overline{V_4}} \overline{f_4} \sqrt{1 - \frac{\overline{V_4^2}}{V_0^2}\sin^2\theta_0},$$

$$a_{7i} = \iota \frac{\omega}{V_i} \sqrt{1 - \frac{V_i^2}{V_0^2}\sin^2\theta_0} f_i, \qquad a_{73} = 0,$$

$$a_{74} = \iota p_2 \frac{\omega}{\overline{\overline{V_4}}} \sqrt{1 - \frac{\overline{V_1^2}}{V_0^2}\sin^2\theta_0} \overline{f_1},$$

$$a_{75} = \iota p_2 \frac{\omega}{\overline{\overline{V_5}}} \sqrt{1 - \frac{\overline{V_2^2}}{V_0^2}\sin^2\theta_0} \overline{f_2},$$

$$a_{76} = a_{77} = 0, \quad (i = 1, 2),$$

$$d_1 = \frac{\lambda}{\rho c_1^2}, \qquad d_2 = \frac{2\mu}{\rho c_1^2}, \qquad d_3 = \frac{d_2}{2},$$

$$d_1^{ff} = \frac{b}{\nu}, \qquad d_1^f = \frac{c_0}{\rho \nu T_0}, \qquad d_2^f = \frac{\lambda^f \omega^*}{\rho c_1^2},$$

$$d_3^f = \frac{\left(2\mu^f + K^f\right)\omega^*}{\rho c_1^2}, \qquad d_4^f = \frac{\mu^f \omega^*}{\rho c_1^2},$$

$$d_5^f = \frac{K^f \omega^*}{\rho c_1^2}, \qquad p_2 = \frac{K_1^*}{K^*},$$

$$c_1 = c_2 = \frac{\nu T_0}{\rho c_1^2}, \qquad c_4 = \frac{\nu c_1^2}{\omega^* K_1^*}. \tag{A.1}$$

Symbols

λ, μ:	Lame's constants
t_{ij}:	Components of the stress tensor
$\vec{u}$:	Displacement vector
ρ:	Density
K^*:	Thermal conductivity
c^*:	Specific heat at constant strain
T_0:	Uniform temperature
T:	Temperature change
α_T:	Coefficient of linear thermal expansion
δ_{ij}:	Kronecker delta
ε_{ijr}:	Alternating symbol
$\lambda^f, \mu^f, K^f,$ $\alpha^f, \beta^f, \gamma^f, c_0$:	Material constants of the fluid
σ_{ij}^f:	Components of stress tensor in the fluid
m_{ij}^f:	Components of couple stress tensor in the fluid
$\vec{v}$:	Velocity vector
$\vec{\Psi}$:	Microrotation velocity vector
ρ^f:	Density
I:	Scalar constant with the dimension of moment of inertia of unit mass
p:	Pressure
K_1^*:	Thermal conductivity
aT_0^f:	Specific heat at constant strain
T_0^f:	Absolute temperature
T^f:	Temperature change
ϕ^{*f}:	Variation in specific volume
α_{T^f}:	Coefficient of linear thermal expansion.

Conflict of Interests

The authors declare that there is no conflict of interests regarding the publication of this paper.

Acknowledgment

Thanks are due to Punjab Technical University, Kapurthala, for providing research facilities and enrolling one of the

authors (Mandeep Kaur) as a research scholar to Ph.D. Programme.

References

[1] A. C. Eringen, "Simple microfluids," *International Journal of Engineering Science*, vol. 2, pp. 205–217, 1964.

[2] A. C. Eringen, "Theory of micropolar fluids," *Journal of Applied Mathematics and Mechanics*, vol. 16, pp. 1–18, 1966.

[3] T. Ariman, M. A. Turk, and N. D. Sylvester, "Microcontinuum fluid mechanics-A review," *International Journal of Engineering Science*, vol. 11, no. 8, pp. 905–930, 1973.

[4] T. Ariman, N. D. Sylvester, and M. A. Turk, "Applications of microcontinuum fluid mechanics," *International Journal of Engineering Science*, vol. 12, no. 4, pp. 273–293, 1974.

[5] P. Říha, "On the theory of heat-conducting micropolar fluids with microtemperatures," *Acta Mechanica*, vol. 23, no. 1-2, pp. 1–8, 1975.

[6] A. C. Eringen and C. B. Kafadar, "Polar field theories," in *Continuum Physics*, A. C. Eringen, Ed., vol. 4, Academic Press, New York, NY, USA, 1976.

[7] O. Brulin, *Linear micropolar media, in Mechanics of Micropolar Media*, edited by O. Brulin and R. K. T. Hsieh, World Scientific, Singapore, 1982.

[8] R. S. R. Gorla, "Combined forced and free convection in the boundary layer flow of a micropolar fluid on a continuous moving vertical cylinder," *International Journal of Engineering Science*, vol. 27, no. 1, pp. 77–86, 1989.

[9] A. C. Eringen, "Theory of thermo-microstretch fluids and bubbly liquids," *International Journal of Engineering Science*, vol. 28, no. 2, pp. 133–143, 1990.

[10] N. U. Aydemir and J. E. S. Venart, "Flow of a thermomicropolar fluid with stretch," *International Journal of Engineering Science*, vol. 28, no. 12, pp. 1211–1222, 1990.

[11] M. Ciarletta, "Spatial decay estimates for heat-conducting micropolar fluids," *International Journal of Engineering Science*, vol. 39, no. 6, pp. 655–668, 2001.

[12] S. Hsia and J. Cheng, "Longitudinal plane wave propagation in elastic-micropolar porous media," *Japanese Journal of Applied Physics*, vol. 45, no. 3, pp. 1743–1748, 2006.

[13] S. Y. Hsia, S. M. Chiu, C. C. Su, and T. H. Chen, "Propagation of transverse waves in elastic-micropolar porous semispaces," *Japanese Journal of Applied Physics*, vol. 46, no. 11, pp. 7399–7405, 2007.

[14] S. K. Tomar and M. L. Gogna, "Reflection and refraction of a longitudinal microrotational wave at an interface between two micropolar elastic solids in welded contact," *International Journal of Engineering Science*, vol. 30, no. 11, pp. 1637–1646, 1992.

[15] S. K. Tomar and M. L. Gogna, "Reflection and refraction of longitudinal wave at an interface between two micropolar elastic solids in welded contact," *Journal of the Acoustical Society of America*, vol. 97, no. 2, pp. 822–830, 1995.

[16] S. K. Tomar and M. L. Gogna, "Reflection and refraction of coupled transverse and micro-rotational waves at an interface between two different micropolar elastic media in welded contact," *International Journal of Engineering Science*, vol. 33, no. 4, pp. 485–496, 1995.

[17] R. Kumar, N. Sharma, and P. Ram, "Reflection and transmission of micropolar elastic waves at an imperfect boundary," *Multidiscipline Modeling in Materials and Structures*, vol. 4, no. 1, pp. 15–36, 2008.

[18] R. Kumar, N. Sharma, and P. Ram, "Interfacial imperfection on reflection and transmission of plane waves in anisotropic micropolar media," *Theoretical and Applied Fracture Mechanics*, vol. 49, no. 3, pp. 305–312, 2008.

[19] D. Singh and S. K. Tomar, "Longitudinal waves at a micropolar fluid/solid interface," *International Journal of Solids and Structures*, vol. 45, no. 1, pp. 225–244, 2008.

[20] Q. Sun, H. Xu, and B. Liang, "Propagation characteristics of longitudinal displacement wave in micropolar fluid with micropolar elastic plate," *Materials Science Forum*, vol. 694, pp. 923–927, 2011.

[21] H. Y. Xu, S. Y. Dang, Q. Y. Sun, and B. Liang, "Reflection and transmission characteristics of coupled wave through micropolar elastic solid interlayer in micropolar fluid," *International Journal of Automation and Power Engineering*, vol. 2, no. 6, pp. 347–354, 2013.

[22] S. Y. Dang, H. Y. Xu, Q. Y. Sun, and B. Liang, "Propagation characteristics of coupled wave through micropolar fluid interlayer in micropolar elastic solid," *Advanced Materials Research*, vol. 721, pp. 729–732, 2013.

[23] C. Fu and P. J. Wei, "The wave propagation through the imperfect interface between two micropolar solids," *Advanced Materials Research*, vol. 803, pp. 419–422, 2013.

[24] K. Sharma and M. Marin, "Reflection and transmission of waves from imperfect boundary between two heat conducting micropolar thermoelastic solids," *Analele Stiintifice ale Universitatii Ovidius Constanta*, vol. 22, pp. 151–175, 2014.

[25] S. K. Vishwakarma, S. Gupta, and A. K. Verma, "Torsional wave propagation in Earth's crustal layer under the influence of imperfect interface," *Journal of Vibration and Control*, vol. 20, no. 3, pp. 355–369, 2014.

[26] H. W. Lord and Y. Shulman, "A generalized dynamical theory of thermoelasticity," *Journal of the Mechanics and Physics of Solids*, vol. 15, no. 5, pp. 299–309, 1967.

[27] A. E. Green and K. A. Lindsay, "Thermoelasticity," *Journal of Elasticity*, vol. 2, no. 1, pp. 1–7, 1972.

[28] A. N. Sinha and S. B. Sinha, "Reflection of thermoelastic waves at a solid half-space with thermal relaxation," *Journal of Physics of the Earth*, vol. 22, no. 2, pp. 237–244, 1974.

[29] S. B. Sinha and K. A. Elsibai, "Reflection of thermoelastic waves at a solid half-space with two relaxation times," *Journal of Thermal Stresses*, vol. 19, no. 8, pp. 749–762, 1996.

[30] H. Deresiewicz, "Effect of boundaries on waves in a thermoelastic solid: reflexion of plane waves from a plane boundary," *Journal of the Mechanics and Physics of Solids*, vol. 8, pp. 164–172, 1960.

[31] R. S. Dhaliwal and A. Singh, *Dynamic Coupled Thermoelasticity*, Hindustan Publication Corporation, New Delhi, India, 1980.

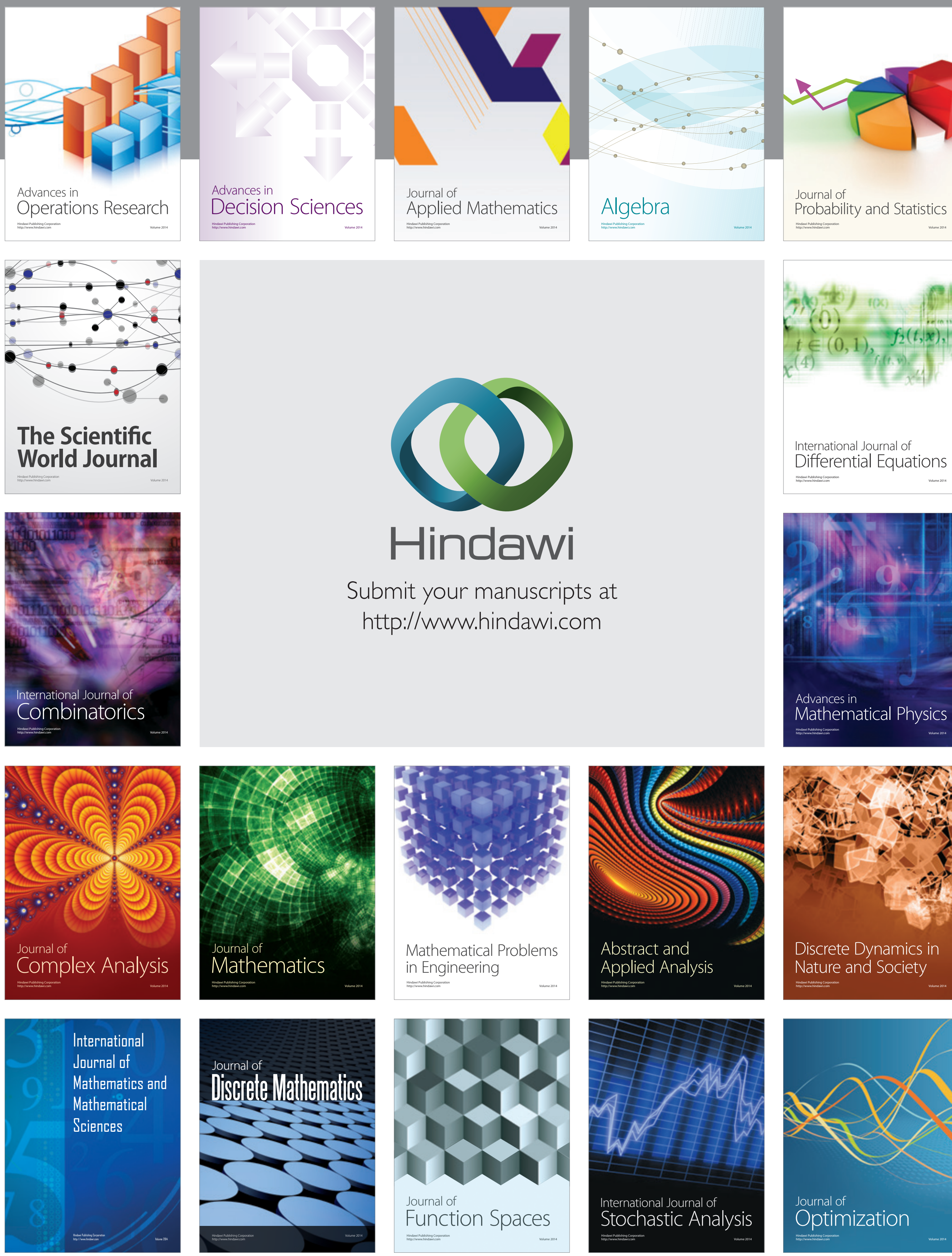
Advances in Operations Research
Advances in Decision Sciences
Journal of Applied Mathematics
Algebra
Journal of Probability and Statistics
The Scientific World Journal
Hindawi
Submit your manuscripts at
http://www.hindawi.com
International Journal of Differential Equations
International Journal of Combinatorics
Advances in Mathematical Physics
Journal of Complex Analysis
Journal of Mathematics
Mathematical Problems in Engineering
Abstract and Applied Analysis
Discrete Dynamics in Nature and Society
International Journal of Mathematics and Mathematical Sciences
Journal of Discrete Mathematics
Journal of Function Spaces
International Journal of Stochastic Analysis
Journal of Optimization